



ELSEVIER

Available online at www.sciencedirect.com

SCIENCE @ DIRECT®

Comput. Methods Appl. Mech. Engrg. 193 (2004) 1085–1103

**Computer methods
in applied
mechanics and
engineering**

www.elsevier.com/locate/cma

An extended meshfree method for boundary value problems

Jiun-Shyan Chen ^{*}, Dongdong Wang, Stanley B. Dong

*Department of Civil & Environmental Engineering, University of California – Los Angeles, 5731G Boelter Hall,
Los Angeles, CA 90095-1593, USA*

Received 6 April 2003; received in revised form 8 September 2003; accepted 4 December 2003

Abstract

An extended meshfree method is presented for treating boundary value problems, where the total solution is expressed by a combination of particular and homogeneous solutions, each of which is assigned a specific role. The particular solution is any analytical (or numerical) expression satisfying the governing differential equation containing the source term but not necessarily the boundary conditions. A general method is presented for constructing this solution. Thus, the problem is reduced to a homogeneous equation where the original boundary conditions are modified by the particular solution. Herein, the meshfree method is used to solve this homogeneous equation, which involves a lower order behavior so that a relatively coarse discretization is acceptable. Several boundary value problems from potential theory as well as from shear deformable plate theory are solved, where linear exactness [Int. J. Numer. Methods Engrg. 50 (2001) 435; Int. J. Numer. Methods Engrg. 53 (2002) 2587] and bending exactness [Comput. Methods Appl. Mech. Engrg. 193 (2004) 1065], respectively, are imposed in their meshfree approximation fields. Numerical results demonstrate that this extended meshfree approach significantly improves the solution accuracy with commensurately less computational effort compared to the conventional meshfree formulation.

© 2004 Elsevier B.V. All rights reserved.

Keywords: Extended meshfree method; Fundamental solution; Auxiliary boundary conditions; Bending exactness; Linear exactness

1. Introduction

Finite element methods and meshfree methods have been widely used for numerical solution of boundary value problems. However, the solution accuracy in these methods is often impaired when there is a localized source term in the partial differential equation (PDE). More specifically, source terms can increase the order of the nonlinear behavior in the solution and thus require a higher order approximation or a finer discretization for an acceptable accuracy.

The unstructured and conforming properties of the meshfree method [2,4,8,14,15] offer tremendous flexibility for enhancement of the local and global solution accuracy. Under the partition of unity

^{*} Corresponding author.

E-mail address: jschen@seas.ucla.edu (J.-S. Chen).

framework [8,15], special enrichment basis functions can be embedded within the Galerkin formulation to better approximate the local behavior. In [1,7] an extended finite element method with enriched basis functions was used to effectively model crack tip characteristics. In [16] a similar approach was employed in thermal and phase change problem. Hierarchical enrichment [12,13,19], coupling between FEM and meshfree methods [9,11,13] and interface enrichment [10,21] were also developed for enhancement of local solutions. These applications attest to the benefit of enriching the trial basis. Enrichment functions for non-localized problems have also been proposed. The work in [17] used a particular solution to satisfy the strong form of the non-homogeneous PDE together with a homogeneous solution using a lower order finite element basis functions. Since lower order finite element basis functions satisfy the differential operator identically, the approximation in the weak form only involves boundary terms after integration-by-parts. This approach possesses the combined advantages of boundary element like features and lower order finite element efficiency.

In this paper, the unknown field variables are decomposed into particular solution and homogeneous solution. We present a general, straightforward approach for constructing the particular solution by employing a fundamental solution that captures the behavior due to the source term in the governing equation without necessarily satisfying the boundary conditions. Consequently, only a homogeneous governing equation with auxiliary boundary conditions remains, which is solved by a meshfree method. By this procedure, the homogeneous solution has a lower order behavior, which can be effectively treated by a stabilized conforming nodal integration (SCNI) [5,6,20] that meets the linear and bending exactness criteria in the Galerkin approximation for potential problem and shear deformable plate problems, respectively. In this study, this version of the extended meshfree method is demonstrated on several boundary value problems from these two problem areas.

This paper is organized as follows. The properties of reproducing kernel approximation and the motivation of this work via a one-dimensional example are summarized in Section 2. In Section 3, a general solution decomposition procedure is presented for a class of boundary values problems. Application of this procedure to Poisson's equation using SCNI for homogeneous solution is presented in Section 4. In Section 5, the proposed method is applied to shear deformable plate problems. Finally, conclusions are drawn in Section 6.

2. Properties of reproducing kernel approximation

The reproducing kernel (RK) approximation [14] is employed herein for the meshfree approximation of the dependent variables in PDEs. The problem domain Ω is first discretized into a set of particles $\{\mathbf{x}_1, \mathbf{x}_2, \dots, \mathbf{x}_{\text{NP}}\}$, where \mathbf{x}_I is the location of node I and NP denotes the total number of particles. The unknown variable $u(\mathbf{x})$ of a PDE is approximated by

$$u^h(\mathbf{x}) = \sum_{I=1}^{\text{NP}} \Psi_I(\mathbf{x}) d_I, \quad (2.1)$$

where $u^h(\mathbf{x})$ is the approximation of $u(\mathbf{x})$, Ψ_I and d_I are the shape functions and their associated coefficients, respectively. In RK approximation [14], a shape function $\Psi_I(\mathbf{x})$ has the form:

$$\Psi_I(\mathbf{x}) = c(\mathbf{x}; \mathbf{x} - \mathbf{x}_I) \phi_a(\mathbf{x} - \mathbf{x}_I), \quad (2.2)$$

where $c(\mathbf{x}; \mathbf{x} - \mathbf{x}_I)$ is the correction function expressed as a linear combination of an n th order monomial basis:

$$c(\mathbf{x}; \mathbf{x} - \mathbf{x}_I) = \mathbf{H}^T(\mathbf{x} - \mathbf{x}_I) \mathbf{b}(\mathbf{x}) \quad (2.3)$$

with vector $\mathbf{H}(\mathbf{x} - \mathbf{x}_I)$ containing the basis functions:

$$\mathbf{H}^T(\mathbf{x} - \mathbf{x}_I) = [1 \quad x_1 - x_{I1} \quad x_2 - x_{I2} \quad (x_1 - x_{I1})^2 \quad \cdots \quad (x_2 - x_{I2})^n]. \tag{2.4}$$

In Eq. (2.2), $\phi_a(\mathbf{x} - \mathbf{x}_I)$ is a kernel function that defines the smoothness and locality of the approximation with a compact support measured by ‘ a ’. A commonly used kernel function is the cubic spline function:

$$\phi_a(r) = \begin{cases} \frac{2}{3} - 4r^2 + 4r^3, & 0 \leq r \leq \frac{1}{2}, \\ \frac{4}{3} - 4r + 4r^2 - \frac{4}{3}r^3, & \frac{1}{2} \leq r \leq 1, \\ 0, & r > 1, \end{cases} \tag{2.5}$$

where $r = \|\mathbf{x} - \mathbf{x}_I\|/a$. The coefficient vector $\mathbf{b}(\mathbf{x})$ in Eq. (2.3) is obtained by satisfying the following n th order reproducing conditions:

$$\sum_{I=1}^{NP} \Psi_I(\mathbf{x}) x_{I1}^\alpha x_{I2}^\beta = x_1^\alpha x_2^\beta, \quad \alpha + \beta = 0, 1, 2, \dots, n. \tag{2.6}$$

The solution for coefficient vector $\mathbf{b}(\mathbf{x})$ is obtained by substituting Eq. (2.2) into Eq. (2.6) to yield:

$$\mathbf{M}(\mathbf{x})\mathbf{b}(\mathbf{x}) = \mathbf{H}(\mathbf{0}), \tag{2.7}$$

$$\mathbf{M}(\mathbf{x}) = \sum_{I=1}^{NP} \mathbf{H}(\mathbf{x} - \mathbf{x}_I)\mathbf{H}^T(\mathbf{x} - \mathbf{x}_I)\phi_{a_I}(\mathbf{x} - \mathbf{x}_I). \tag{2.8}$$

Upon solving for $\mathbf{b}(\mathbf{x}) = \mathbf{M}^{-1}(\mathbf{x})\mathbf{H}(\mathbf{0})$, the RK shape functions take the form:

$$\Psi_I(\mathbf{x}) = \mathbf{H}^T(\mathbf{0})\mathbf{M}^{-1}(\mathbf{x})\mathbf{H}(\mathbf{x} - \mathbf{x}_I)\phi_a(\mathbf{x} - \mathbf{x}_I). \tag{2.9}$$

The reproducing kernel particle method (RKPM) is formulated by introducing the above approximation of unknown into the weak form of the governing equation $\mathcal{L}[u] + b = 0$ where \mathcal{L} is the differential operator and b is the source term. The order of the solution is greatly dependent upon the nature of source term and

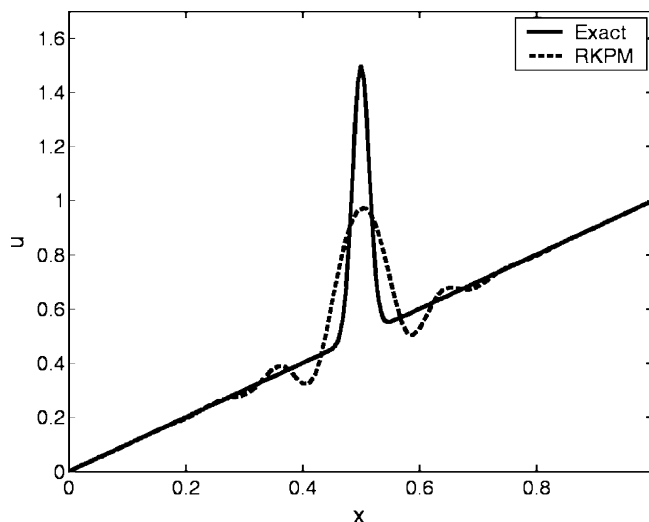


Fig. 1. Exact and meshfree solutions in 1D with localization.

the differential operator. The following problem illustrates the property of the conventional Galerkin meshfree method using the reproducing kernel approximation with linear basis and 20-node discretization in representing the behavior of a localized high-gradient source term:

$$\begin{aligned} u_{,xx} + b(x) &= 0 \quad \text{in } (0, 1), \\ b(x) &= \begin{cases} \{2\alpha^2 - 4[\alpha^2(x - 0.5)]^2\} \exp\{-[\alpha(x - 0.5)]^2\} & \text{for } 0.42 \leq x \leq 0.58, \\ 0 & \text{otherwise,} \end{cases} \\ u(0) &= 0, \quad u(1) = 1, \quad \alpha = 50. \end{aligned} \quad (2.10)$$

A comparison of the numerical and exact solutions in Fig. 1 shows very significant differences in the vicinity of the localized source term.

3. Extended meshfree method

To illustrate the extended meshfree method, consider the following one-dimensional model problem:

$$\begin{aligned} u_{,xx} + b(x) &= 0 \quad \text{in } (a, b), \\ u(a) &= \bar{u}_a, \quad u(b) = \bar{u}_b. \end{aligned} \quad (3.1)$$

The solution can be expressed by means of Green's function as $u(x) = \int_a^b \hat{g}(x, y)b(y) dy + [(b - x)\bar{u}_a + (x - a)\bar{u}_b]/(b - a)$, where Green's function $\hat{g}(x, y)$ satisfies $\hat{g}_{,xx} + \delta(x - y) = 0$ in (a, b) , and boundary conditions $\hat{g}(a, y) = 0$, $\hat{g}(b, y) = 0$. However, a Green's function may not always be available in general problems. Rather than seeking a Green's function, consider an alternate function g that satisfies governing equation (3.1) in an infinite domain but perhaps not the boundary conditions. Such a fundamental solution can be easily constructed. For governing equation (3.1), let g satisfy the following equation in an infinite domain:

$$g_{,xx} + \delta(x - \bar{x}) = 0. \quad (3.2)$$

The solution of (3.2) has the form

$$g(x, \bar{x}) = \begin{cases} x, & x \leq \bar{x}, \\ \bar{x}, & x > \bar{x}. \end{cases} \quad (3.3)$$

With this form of $g(x, \bar{x})$, a particular solution to Eq. (3.1) can be obtained by

$$u^p(x) = \int_a^b g(x, y)b(y) dy, \quad (3.4)$$

where $u^p(x)$ does not generally satisfy the boundary conditions in Eq. (3.1). With $u^p(x)$ given by Eq. (3.4), the total solution can then be taken as

$$u(x) = u^0(x) + u^p(x), \quad (3.5)$$

where $u^0(x)$ is the homogeneous solution satisfying the following homogeneous equation with boundary conditions modified by the particular solution:

$$\begin{aligned} u_{,xx}^0 &= 0 \quad \text{in } (a, b), \\ u^0(a) &= \bar{u}_a - u^p(a), \quad u^0(b) = \bar{u}_b - u^p(b). \end{aligned} \quad (3.6)$$

The variable $u^0(x)$ of Eq. (3.6) without a source term involves a lower order behavior compared to the original problem, and its analysis can be treated numerically with greater ease.

This approach can be generalized to treat a multi-dimensional boundary value problems with mixed boundary conditions. Consider the problem:

$$\begin{aligned} \mathcal{L}[u] + b(\mathbf{x}) &= 0 \quad \text{in } \Omega, \\ u &= p \quad \text{on } \partial_u\Omega, \\ \frac{\partial u}{\partial n} &= h \quad \text{on } \partial_h\Omega. \end{aligned} \tag{3.7}$$

Let $g(\mathbf{x}, \bar{\mathbf{x}})$ be the fundamental solution that satisfies

$$\mathcal{L}[g] + \delta(\mathbf{x} - \bar{\mathbf{x}}) = 0, \tag{3.8}$$

where $\delta(\mathbf{x} - \bar{\mathbf{x}})$ is a multi-dimensional delta function. Then a particular solution is given by the integral:

$$u^p(\mathbf{x}) = \int_{\Omega} g(\mathbf{x}, \mathbf{y}) b(\mathbf{y}) \, d\mathbf{y}. \tag{3.9}$$

The homogeneous solution $u^0(\mathbf{x})$ is then obtained from the homogeneous equation with boundary conditions modified by $u^p(\mathbf{x})$:

$$\begin{aligned} \mathcal{L}[u^0] &= 0 \quad \text{in } \Omega, \\ u^0 &= p - u^p \equiv p^0 \quad \text{on } \partial_u\Omega, \\ \frac{\partial u^0}{\partial n} &= h - h^p \equiv h^0 \quad \text{on } \partial_h\Omega, \end{aligned} \tag{3.10}$$

where $h^p(\mathbf{x}) = \frac{\partial u^p}{\partial n} = \int_{\Omega} \frac{\partial g(\mathbf{x}, \mathbf{y})}{\partial n} b(\mathbf{y}) \, d\mathbf{y}$, $\mathbf{x} \in \partial_h\Omega$. Specific solution procedures for Poisson’s equation as well as plate bending problems are discussed in the following two sections.

4. Poisson’s equation

4.1. Model problem and fundamental solution

Consider the following Poisson equation in two dimensions:

$$\begin{aligned} \nabla^2 u + b(\mathbf{x}) &= 0 \quad \text{in } \Omega, \\ u &= p \quad \text{on } \partial_u\Omega, \quad \frac{\partial u}{\partial n} = h \quad \text{on } \partial_h\Omega, \end{aligned} \tag{4.1}$$

where $\partial_u\Omega$ and $\partial_h\Omega$ denote the essential and natural boundaries, respectively, $\partial_u\Omega \cup \partial_h\Omega = \partial\Omega$, $\partial_u\Omega \cap \partial_h\Omega = \emptyset$, and \mathbf{n} denotes the outward normal to the boundary. The fundamental solution satisfies

$$\nabla^2 g + \delta(\mathbf{x} - \bar{\mathbf{x}}) = 0 \tag{4.2}$$

and its solution is [3,22]

$$g(\mathbf{x}, \bar{\mathbf{x}}) = -\frac{1}{2\pi} \ln r, \quad r = \|\bar{\mathbf{x}} - \mathbf{x}\| = [(\bar{x} - x)^2 + (\bar{y} - y)^2]^{1/2}. \tag{4.3}$$

The particular solution that accounts for $b(\mathbf{x})$ is obtained by Eq. (3.9).

4.2. Linear exactness in approximation of homogeneous solution

The homogeneous solution must satisfy the following equation and boundary conditions:

$$\begin{aligned}
 \nabla^2 u^0 &= 0 \quad \text{in } \Omega, \\
 u^0 &= p - u^p \equiv p^0 \quad \text{on } \partial_u \Omega, \\
 \frac{\partial u^0}{\partial n} &= h - \frac{\partial u^p}{\partial n} \equiv h^0 \quad \text{on } \partial_h \Omega.
 \end{aligned}
 \tag{4.4}$$

The weak form of (4.4) is

$$\int_{\Omega} \nabla \delta u^0 \cdot \nabla u^0 \, dA = \int_{\partial_h \Omega} \delta u^0 h^0 \, d\Gamma.
 \tag{4.5}$$

Following [5,6], the necessary conditions for achieving linear exactness in the Galerkin approximation of this second order differential equation are: (1) shape functions Ψ_I for approximation of the unknown $u^{0h}(\mathbf{x}) = \sum_I \Psi_I(\mathbf{x}) d_I^0$ are linearly complete, and (2) integration of the weak form meets integration constraints.

These requirements are met by employing linear basis functions in the reproducing kernel approximation and by satisfying integration constraints given in [5] as

$$\text{Int}_{\Omega}(\nabla \Psi_I) = \int_{\partial_h \Omega} \Psi_I \mathbf{n} \, d\Gamma \quad \text{for } \{I : \text{supp}(\Psi_I) \cap \partial_u \Omega = \emptyset\},
 \tag{4.6}$$

where $\text{Int}_{\Omega}(\cdot)$ denotes numerical integration over domain Ω . A SCNI has been proposed to stabilize the nodal integration of the weak form and fulfill linear exactness in the Galerkin approximation of second order differential equation [5]. In this approach, a smoothed nodal gradient of u^0 at point \mathbf{x}_L is computed as

$$\tilde{\nabla} u^{0h}(\mathbf{x}_L) = \frac{1}{A_L} \int_{\Omega_L} \nabla u^{0h} \, dA = \frac{1}{A_L} \int_{\Gamma_L} \mathbf{m} u^{0h} \, d\Gamma = \sum_I \tilde{\nabla} \Psi_I(\mathbf{x}_L) d_I^0,
 \tag{4.7}$$

where

$$\tilde{\nabla} \Psi_I(\mathbf{x}_L) = \frac{1}{A_L} \int_{\Gamma_L} \Psi_I(\mathbf{x}) \mathbf{n}(\mathbf{x}) \, d\Gamma.
 \tag{4.8}$$

Here Ω_L and Γ_L are the representative domain and boundary associated with the node L as shown in Fig. 2, and A_L is the area of Ω_L . It can be easily shown that this smoothed gradient meets the integration constraints for nodal integration:

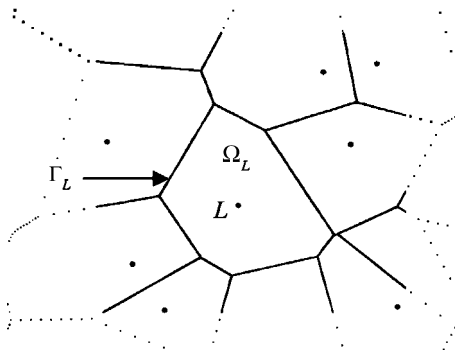


Fig. 2. Nodal representative domain obtained by Voronoi diagram.

$$\sum_{I=1}^{NP} \tilde{\nabla} \Psi_I(\mathbf{x}_K) A_K = \int_{\partial_n \Omega} \Psi_I \mathbf{n} d\Gamma \quad \text{for } \{I : \text{supp}(\Psi_I) \cap \partial_u \Omega = \emptyset\}. \tag{4.9}$$

Introducing a nodal integration of weak form in Eq. (4.5) with assumed gradient field yields

$$\sum_{L=1}^{NP} \tilde{\nabla} \delta u^0(\mathbf{x}_L) \tilde{\nabla} u^0(\mathbf{x}_L) A_L = \sum_{K=1}^{NB_{\text{int}}} \delta u^0(\bar{\mathbf{x}}_K) h^0(\bar{\mathbf{x}}_K) \varpi_K, \tag{4.10}$$

where NP and NB_{int} are, respectively, the numbers of nodal points and boundary integration points, and $\bar{\mathbf{x}}_K$ and ϖ_K are the integration points and weights for boundary integration, respectively, that are consistent with the boundary integration for gradient smoothing term $\int_{\Gamma_L} \Psi_I(\mathbf{x}) \mathbf{n}(\mathbf{x}) d\Gamma$ in Eq. (4.8). By substituting the meshfree approximation for u^0 in Eq. (2.1) into Eq. (4.7), we obtain the following discrete homogeneous equation:

$$\mathbf{K} \mathbf{d}^0 = \mathbf{f}^0, \tag{4.11}$$

$$K_{IJ} = \sum_{L=1}^{NP} \tilde{\nabla} \Psi_I(\mathbf{x}_L) \cdot \tilde{\nabla} \Psi_J(\mathbf{x}_L) A_L, \tag{4.12}$$

$$f_I^0 = \sum_{K=1}^{NB_{\text{int}}} \Psi_I(\bar{\mathbf{x}}_K) h^0(\bar{\mathbf{x}}_K) \varpi_K. \tag{4.13}$$

4.3. Numerical examples

In this subsection, the solutions obtained using RKPM and the proposed extended reproducing kernel particle method (Extended-RKPM) are compared. Both methods employ SCNI for enhanced solution accuracy. For Poisson’s equation, reproducing kernel with linear basis is used.

4.3.1. One-dimensional problem

Problem (2.10) is reconsidered by the extended meshfree method, where the discretization used for the homogeneous problem with modified boundary conditions is the same as before. The particular solution in this case is carried out by three integration zones with 6-point quadrature rule in the small domain where $b(x) \neq 0$, and the homogeneous solution is obtained by RKPM with SCNI. Note that this homogeneous solution solved by RKPM with SCNI is exact with arbitrary discretization (3-node discretization is used herein). The comparison of the results in Fig. 3 shows a remarkable improvement in solution accuracy with the Extended-RKPM.

4.3.2. Two-dimensional problem

Poisson’s equation (4.1) with the following source term is analyzed to study the convergence behavior of proposed formulation:

$$b(\mathbf{x}) = -1 - 3y + \{2(\alpha^2 + \beta^2) - 4[\alpha^2(x - 0.5)]^2 - 4[\beta^2(y - 0.5)]^2\} \times \exp\{-[\alpha(x - 0.5)]^2 - [\beta(y - 0.5)]^2\},$$

$$\alpha = \beta = 20. \tag{4.14}$$

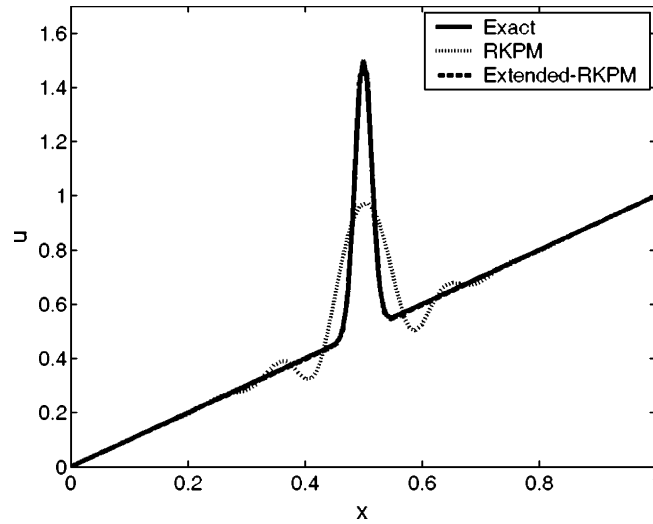


Fig. 3. Extended-RKPM solution of problem (2.10).

The boundary conditions are prescribed as follows:

$$u(x = 0, y) = \frac{y^2}{2} + \exp \left\{ -\frac{\alpha^2}{4} - [\beta(y - 0.5)]^2 \right\}, \tag{4.15}$$

$$u(x = 1, y) = \frac{1 + y^3}{2} + \exp \left\{ -\frac{\alpha^2}{4} - [\beta(y - 0.5)]^2 \right\}, \tag{4.16}$$

$$u(x, y = 0) = \frac{x^2}{2} + \exp \left\{ -[\alpha(x - 0.5)]^2 - \frac{\beta^2}{4} \right\}, \tag{4.17}$$

$$u(x, y = 1) = \frac{x^2 + y^3}{2} + \exp \left\{ -[\alpha(x - 0.5)]^2 - \frac{\beta^2}{4} \right\}. \tag{4.18}$$

The exact solution is given by the following equation and shown graphically in Fig. 4:

$$u(\mathbf{x}) = \frac{x^2 + y^3}{2} + \exp \{ -[\alpha(x - 0.5)]^2 - [\beta(y - 0.5)]^2 \}. \tag{4.19}$$

Here, the particular solution was calculated using a 7×7 Gauss quadrature in the small domain where $b(\mathbf{x}) \neq 0$. The numerical solutions for both Extended-RKPM and RKPM, using both 5×5 and 9×9 discretizations, are plotted in Figs. 5 and 6, respectively. The comparison of these two figures shows that an accurate solution can be obtained by the proposed Extended-RKPM even with a relatively coarse discretization. Moreover, the results using the conventional RKPM method do not compare well even with the most refined 9×9 mesh. The L2 error norms in Fig. 7 demonstrate a significant improvement of accuracy of the proposed method compared to the conventional method, although the rates of convergence of both approaches are comparable.

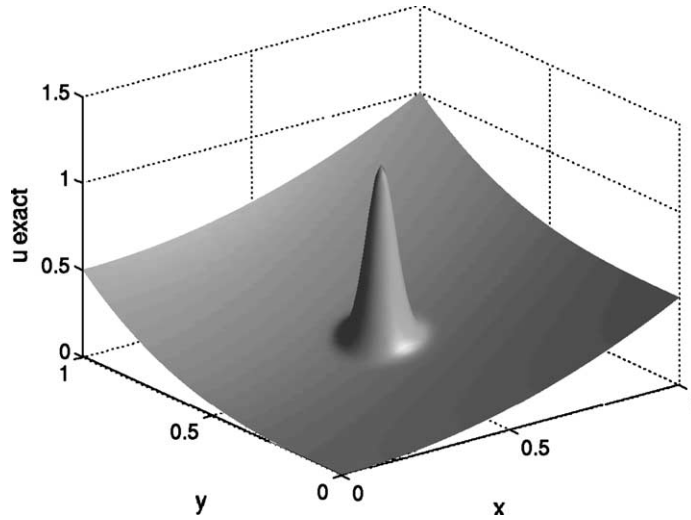


Fig. 4. Exact solution of Poisson's problem with localized source term.

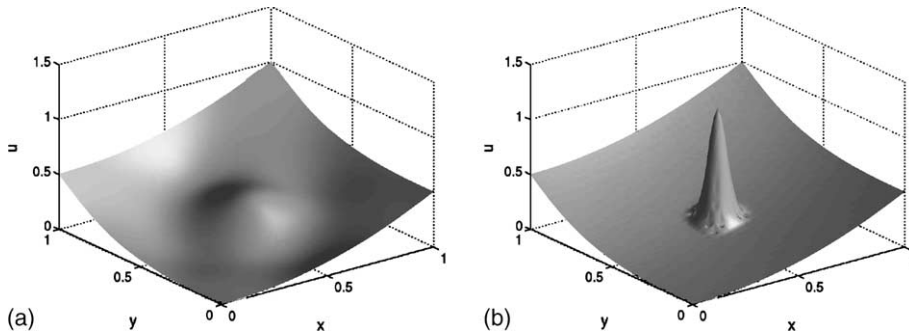


Fig. 5. Solution comparison with 5×5 discretization: (a) RKPM; (b) Extended-RKPM in Poisson's problem with localized source term.

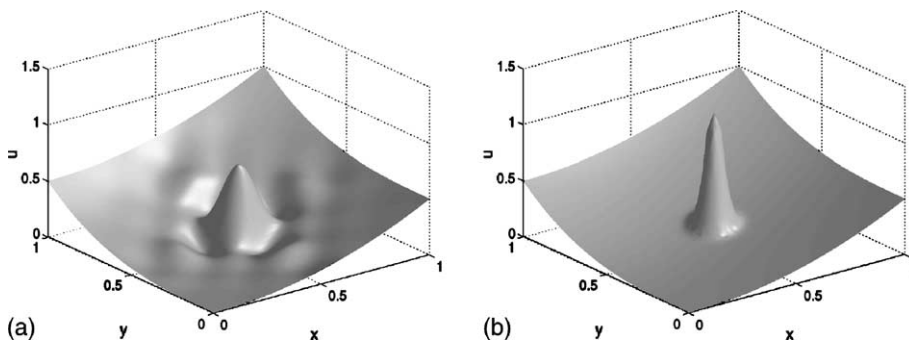


Fig. 6. Solution comparison with 9×9 discretization: (a) RKPM; (b) Extended-RKPM Poisson's problem with localized source term.

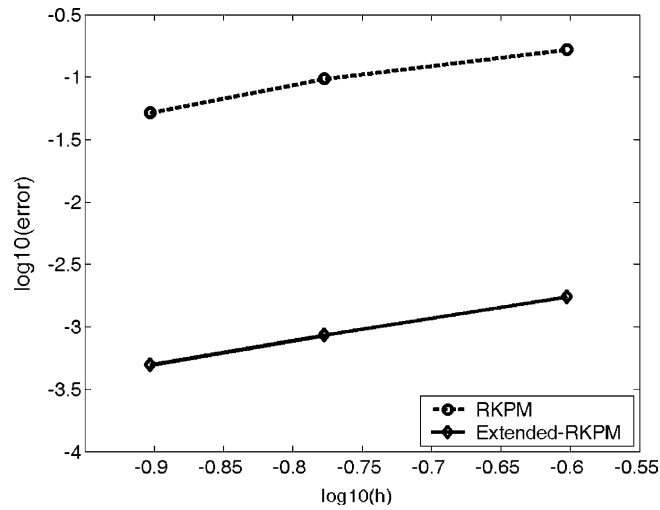


Fig. 7. L2 error norm comparison for Poisson’s problem with localized source term.

5. Shear deformable plate

5.1. Model problem and fundamental solution

The governing equations for Mindlin–Reissner plate theory can be expressed in terms of the transverse displacement w and bending rotations θ_x ’s as

$$D \left(\frac{1-\nu}{2} \nabla^2 \theta_x + \frac{1+\nu}{2} \theta_{\beta,\beta x} \right) + C(w_{,x} - \theta_x) = 0, \tag{5.1}$$

$$C(\nabla^2 w - \theta_{x,x}) + q = 0, \tag{5.2}$$

where $C = \frac{5}{6} \frac{Et}{2(1+\nu)}$, $D = \frac{Et^3}{12(1-\nu^2)}$, E and ν are Young’s modulus and Poisson’s ratio, t is the plate thickness, q is transverse loading, and α and β range from 1 and 2. The sign convention of the rotations is shown in Fig. 8.

Consider a point load $q = \delta(x - \bar{x})$ acting at point \bar{x} in an infinite domain (Fig. 9). The fundamental solutions of Eq. (5.2) due to $q = \delta(x - \bar{x})$ are [22]:

$$w^*(\mathbf{x}, \bar{\mathbf{x}}) = \frac{1}{8\pi D} r^2 \ln r - \frac{1}{2\pi C} \ln r; \quad r = \|\bar{\mathbf{x}} - \mathbf{x}\| = [(\bar{x} - x)^2 + (\bar{y} - y)^2]^{1/2}, \tag{5.3}$$

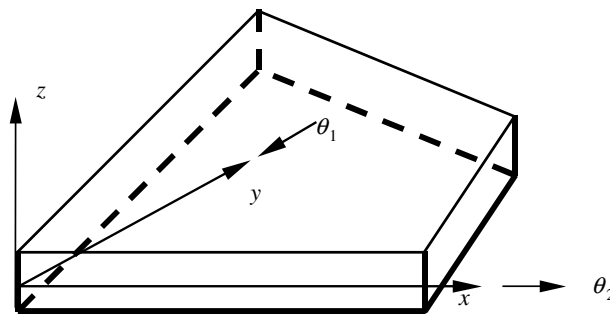


Fig. 8. Sign convention for Mindlin–Reissner plate.

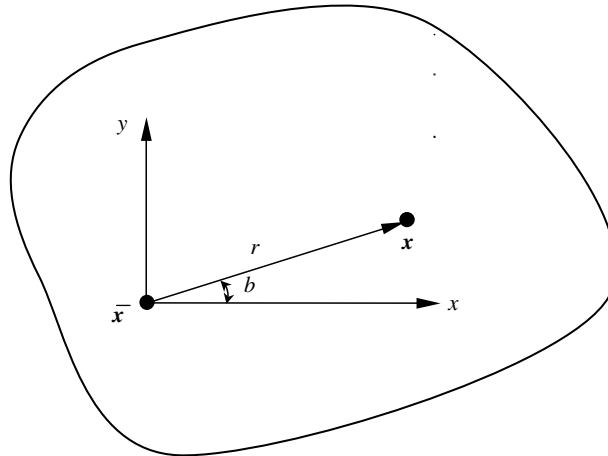


Fig. 9. Point load in an infinite domain.

$$\theta_x^*(\mathbf{x}, \bar{\mathbf{x}}) = \frac{1}{8\pi D} r(2 \ln r + 1) \cos b, \tag{5.4}$$

$$\theta_y^*(\mathbf{x}, \bar{\mathbf{x}}) = \frac{1}{8\pi D} r(2 \ln r + 1) \sin b. \tag{5.5}$$

5.2. Bending exactness in homogeneous solution

Decompose the dependent variables by $w = w^p + w^0$, $\theta_z = \theta_z^p + \theta_z^0$, where w^p and θ_z^p are the particular solution given by $w^p(\mathbf{x}) = \int_{\Omega} w^*(\mathbf{x}, \mathbf{y})q(\mathbf{y}) d\mathbf{y}$ and $\theta_z^p(\mathbf{x}) = \int_{\Omega} \theta_z^*(\mathbf{x}, \mathbf{y})q(\mathbf{y}) d\mathbf{y}$. Thus, only the homogeneous solution remains where the governing equations are the same as Eqs. (5.1) and (5.2) except with the absence of loading term q . The auxiliary boundary conditions can also be obtained with the same procedures as discussed in the previous sections.

The weak form of this auxiliary Mindlin–Reissner plate problem can be expressed as

$$\int_{\Omega} \delta \boldsymbol{\kappa}^{0T} \mathbf{D}^b \boldsymbol{\kappa}^0 d\Omega + \int_{\Omega} \delta \boldsymbol{\gamma}^{0T} \mathbf{D}^s \boldsymbol{\gamma}^0 d\Omega + \int_{\Gamma^h} \delta \boldsymbol{\theta}^{0T} \mathbf{M}^0 d\Gamma = 0, \tag{5.6}$$

where \mathbf{M}^0 is the modified boundary bending moment and other matrices are defined as follows:

$$\mathbf{D}^b = \frac{Et^3}{12(1 - \nu^2)} \begin{pmatrix} 1 & \nu & 0 \\ \nu & 1 & 0 \\ 0 & 0 & (1 - \nu)/2 \end{pmatrix}, \quad \mathbf{D}^s = tk\mu \begin{pmatrix} 1 & 0 \\ 0 & 1 \end{pmatrix}, \tag{5.7}$$

$$\boldsymbol{\kappa}^0 = \begin{pmatrix} k_{11}^0 \\ k_{22}^0 \\ 2k_{12}^0 \end{pmatrix} = \begin{pmatrix} \frac{\partial \theta_1^0}{\partial x_1} \\ \frac{\partial \theta_2^0}{\partial x_2} \\ \frac{\partial \theta_1^0}{\partial x_2} + \frac{\partial \theta_2^0}{\partial x_1} \end{pmatrix}, \quad \boldsymbol{\gamma}^0 = \begin{pmatrix} \gamma_1^0 \\ \gamma_2^0 \end{pmatrix} = \begin{pmatrix} w_{,1}^0 - \theta_1^0 \\ w_{,2}^0 - \theta_2^0 \end{pmatrix}. \tag{5.8}$$

To avoid shear locking in the limit as $t \rightarrow 0$, the homogeneous system of equations must be solved using a reproducing kernel approximation of unknowns that meet (1) Krichhoff mode reproducing conditions (KMRC), and (2) the bending exactness (BE) in the Galerkin approximation of Mindlin–Reissner plate [20]. To satisfy KMRC, a reproducing kernel approximation with quadratic basis for w^0 and θ_x^0 is employed:

$$\mathbf{u}^{0h} = \begin{pmatrix} w^{0h} \\ \theta_1^{0h} \\ \theta_2^{0h} \end{pmatrix} = \sum_{I=1}^{NP} \Psi_I \begin{pmatrix} w_I^0 \\ \theta_{1I}^0 \\ \theta_{2I}^0 \end{pmatrix} = \sum_{I=1}^{NP} \Psi_I(\mathbf{x}) \mathbf{d}_I^0, \tag{5.9}$$

where Ψ_I is the RK shape function constructed with second order basis functions. The corresponding approximation of shear strain and curvature are

$$\boldsymbol{\gamma}^{0h} = \begin{pmatrix} \gamma_1^{0h} \\ \gamma_2^{0h} \end{pmatrix} = \sum_{I=1}^{NP} \begin{pmatrix} \Psi_{I,1} w_I^0 - \Psi_I \theta_{1I}^0 \\ \Psi_{I,2} w_I^0 - \Psi_I \theta_{2I}^0 \end{pmatrix} = \sum_{I=1}^{NP} \mathbf{B}_I^s \mathbf{d}_I^0, \tag{5.10}$$

$$\boldsymbol{\kappa}^{0h} = \begin{pmatrix} \kappa_{11}^{0h} \\ \kappa_{22}^{0h} \\ 2\kappa_{12}^{0h} \end{pmatrix} = \begin{pmatrix} \frac{\partial \theta_1^{0h}}{\partial x_1} \\ \frac{\partial \theta_2^{0h}}{\partial x_2} \\ \frac{\partial \theta_1^{0h}}{\partial x_2} + \frac{\partial \theta_2^{0h}}{\partial x_1} \end{pmatrix} = \sum_{I=1}^{NP} \begin{pmatrix} \Psi_{I,1} \theta_{1I}^0 \\ \Psi_{I,2} \theta_{2I}^0 \\ \Psi_{I,2} \theta_{1I}^0 + \Psi_{I,1} \theta_{2I}^0 \end{pmatrix} = \sum_{I=1}^{NP} \mathbf{B}_I^b \mathbf{d}_I^0, \tag{5.11}$$

where

$$\mathbf{B}_I^b = \begin{pmatrix} 0 & \Psi_{I,x} & 0 \\ 0 & 0 & \Psi_{I,y} \\ 0 & \Psi_{I,y} & \Psi_{I,x} \end{pmatrix}; \quad \mathbf{B}_I^s = \begin{pmatrix} \Psi_{I,x} & -\Psi_I & 0 \\ \Psi_{I,y} & 0 & -\Psi_I \end{pmatrix}. \tag{5.12}$$

To fulfill BE, numerical integration for the weak form must satisfy the following integration constraint:

$$\int_{\Omega} \mathbf{B}_I^{bT} d\Omega = \int_{\Gamma^h} \mathbf{E}_I^T d\Gamma \quad \text{for } \{I : \text{supp}(\Psi_I) \cap \partial_u \Omega = \emptyset\}, \tag{5.13}$$

where $\partial_u \Omega$ is the essential boundary of the plate, and

$$\mathbf{E}_I = \begin{pmatrix} 0 & \Psi_I n_1 & 0 \\ 0 & 0 & \Psi_I n_2 \\ 0 & \Psi_I n_2 & \Psi_I n_1 \end{pmatrix}. \tag{5.14}$$

To meet integration constraint and provide stability to the nodally integrated weak form, a curvature smoothing at the nodal point is introduced:

$$\tilde{\kappa}_{\alpha\beta}^0(\mathbf{x}_L) = \frac{1}{A_L} \int_{\Omega_L} \kappa_{\alpha\beta}^0(\mathbf{x}) dA = \frac{1}{2A_L} \int_{\Omega_L} (\theta_{\alpha,\beta}^0 + \theta_{\beta,\alpha}^0) dA = \frac{1}{2A_L} \int_{\Gamma_L} (\theta_\alpha^0 n_\beta + \theta_\beta^0 n_\alpha) d\Gamma, \tag{5.15}$$

$$\kappa^0(\mathbf{x}_L) = \sum_{I=1}^{NP} \tilde{\mathbf{B}}_I^b(\mathbf{x}_L) \mathbf{d}_I^0; \quad \tilde{\mathbf{B}}_I^b(\mathbf{x}_L) = \begin{pmatrix} 0 & \tilde{\Psi}_{I,1}(\mathbf{x}_L) & 0 \\ 0 & 0 & \tilde{\Psi}_{I,2}(\mathbf{x}_L) \\ 0 & \tilde{\Psi}_{I,2}(\mathbf{x}_L) & \tilde{\Psi}_{I,1}(\mathbf{x}_L) \end{pmatrix}; \quad \tilde{\Psi}_{I,\alpha}(\mathbf{x}_L) = \frac{1}{A_L} \int_{\Gamma_L} \Psi_I(\mathbf{x}) n_\alpha(\mathbf{x}) d\Gamma. \tag{5.16}$$

By performing nodal integration of weak form with the above smoothed curvature, we have

$$\sum_{K=1}^{NP} (\delta \tilde{\mathbf{k}}^{0T}(\mathbf{x}_L) \mathbf{D}^b \tilde{\mathbf{k}}^0(\mathbf{x}_L) + \delta \gamma^{0T}(\mathbf{x}_L) \mathbf{D}^s \gamma^0(\mathbf{x}_L)) A_L = - \sum_{K=1}^{NB_{\text{int}}} (\delta \theta^{0T}(\bar{\mathbf{x}}_K) \mathbf{M}^0(\bar{\mathbf{x}}_K)) \varpi_K. \tag{5.17}$$

This leads to the following discrete equation:

$$(\mathbf{K}^b + \mathbf{K}^s) \mathbf{d}^0 = \mathbf{f}^0, \tag{5.18}$$

where

$$\mathbf{K}_{IJ}^b = \sum_{K=1}^{NP} \tilde{\mathbf{B}}_I^{bT}(\mathbf{x}_L) \mathbf{D}^b \tilde{\mathbf{B}}_J^b(\mathbf{x}_L) A_L, \tag{5.19}$$

$$\mathbf{K}_{IJ}^s = \sum_{K=1}^{NP} \mathbf{B}_I^T(\mathbf{x}_L) \mathbf{D}^s \mathbf{B}_J(\mathbf{x}_L) A_L, \tag{5.20}$$

$$\mathbf{f}_I^0 = \sum_{K=1}^{NB_{\text{int}}} \Psi_I(\bar{\mathbf{x}}_K) \begin{pmatrix} 0 \\ -M_x^0(\bar{\mathbf{x}}_K) \\ -M_y^0(\bar{\mathbf{x}}_K) \end{pmatrix} \varpi_K, \tag{5.21}$$

where \mathbf{K}^b and \mathbf{K}^s denote the bending and shear stiffnesses, respectively, NB_{int} is the number of boundary integration points, and $\bar{\mathbf{x}}_K$ and ϖ_K are the integration points and weight of boundary integration, respectively.

5.3. Numerical examples

In this section, results for the Mindlin–Reissner plate problem by RKPM and Extended-RKPM, both using SCNI, are compared. Reproducing kernel approximation with quadratic basis is employed to preserve Kirchhoff mode so that shear locking is avoided.

5.3.1. Clamped circular plate

A clamped circular plate subjected to a unit concentrated load P at the plate centroid is analyzed (Fig. 10). The relevant plate properties are Poisson’s ratio $\nu = 0.3$ and thickness/radius ratio $t/R = 0.02$. Due to axisymmetry, a quarter model is used, whose discretization and corresponding nodes for performing stabilized conforming nodal integration are shown in Fig. 11. Since the source term is due to a point load, the particular solution is the fundamental solution. To study the numerical solution accuracy, it is noted that a singularity exists in the Mindlin–Reissner analytical solution, whereas Kirchhoff analytical solution exhibits no singularity under a point load. In the case of thin plate with $t/R = 0.02$ in Fig 12, Kirchhoff and Mindlin–Reissner solutions are almost identical except within $r/R < 10^{-6}$ as shown in Fig. 13. Good

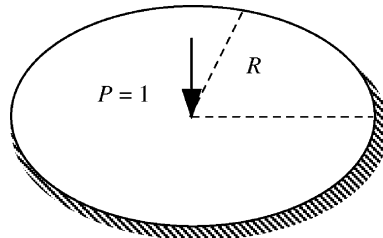


Fig. 10. Clamped plate subjected to a point load.

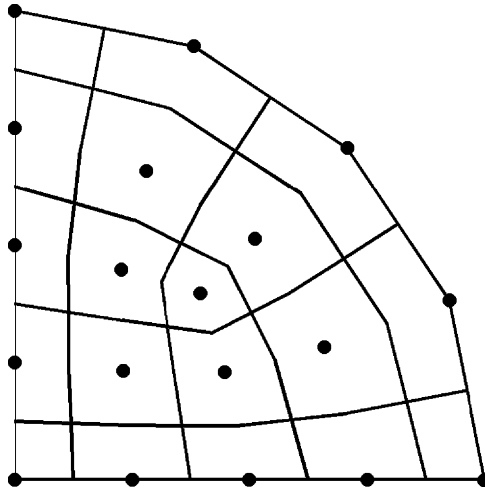
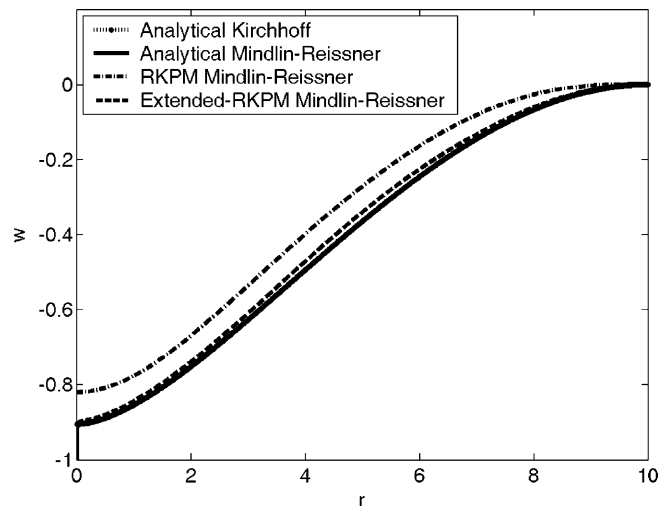


Fig. 11. Discretization of a quarter of circular plate.

Fig. 12. Deflection of clamped circular plate with $t/R = 0.02$.

accuracy of extended-RKPM Mindlin-Reissner solution is shown not only in Fig. 12, but also in the vicinity of point load shown in Fig. 13 where the singularity of the Mindlin-Reissner solution is well captured. To avoid evaluation at a singular point, the normalized deflection of RKPM and proposed Extended-RKPM are computed at $r = 10^{-4}R$ and the results are shown in Fig. 14. The results clearly demonstrate the superior performance of the proposed approach over the conventional meshfree method. For the thick plate case with $t/R = 0.2$ as shown in Fig. 15, Mindlin-Reissner plate analytical solution is substantially different from the Kirchhoff analytical solution. Again, the Extended-RKPM Mindlin-Reissner solution agrees with the Mindlin-Reissner analytical solution much better than that of the conventional RKPM. A dramatic enhancement in Extended-RKPM over RKPM in capturing the highly

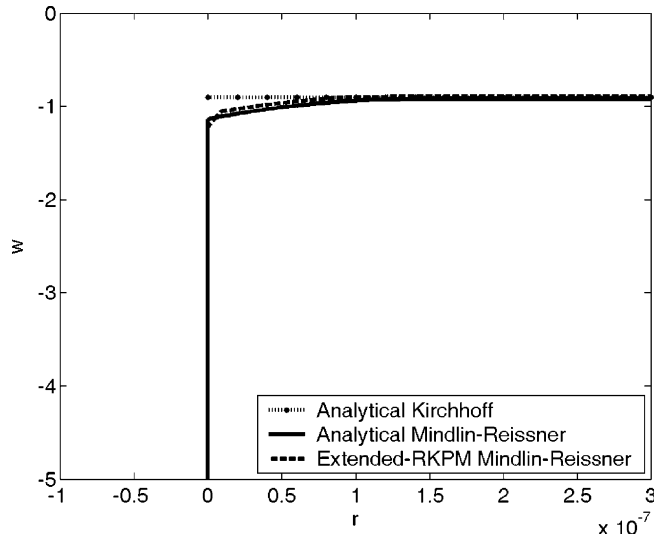


Fig. 13. Deflection of clamped circular plate near plate centroid (zoom-in plot).

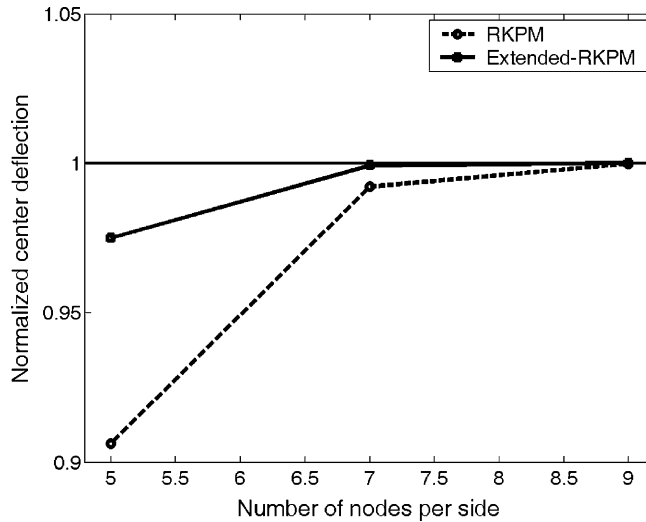


Fig. 14. Center deflection of clamped circular plate.

nonlinear moment distribution in the radial direction is shown in Fig. 16. The improved accuracy in the proposed method can also be observed in the L2 error norm plot in Fig. 17.

5.3.2. Clamped square plate

Consider a clamped square plate of side dimension a under a point force P at the center as shown in Fig. 18. The relevant plate properties for this example are Poisson’s ratio $\nu = 0.3$ and thickness/side ratio $t/a = 0.01$. Again, no numerical integration is needed for the particular solution as the fundamental solution represents the response due to the point load. Similar to the circular plate problem, to avoid the

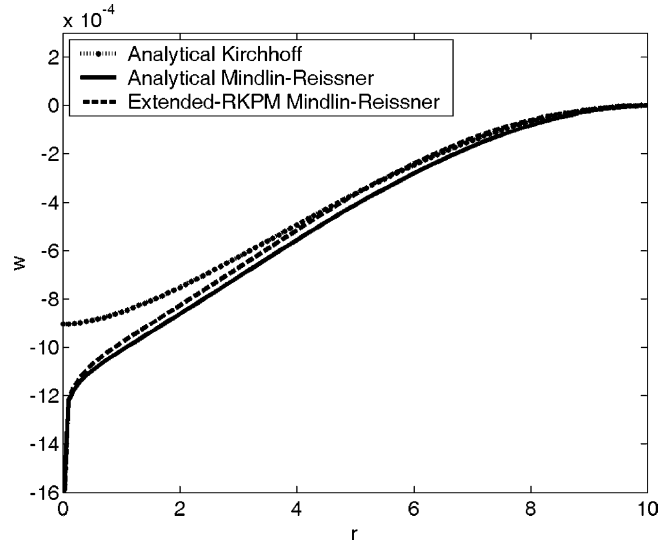


Fig. 15. Deflection of clamped circular plate with $t/R = 0.2$.

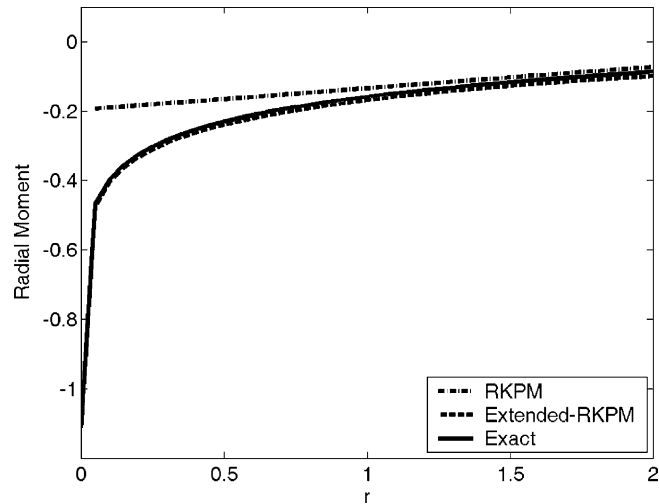


Fig. 16. Comparison of moment distribution along radial direction in clamped circular plate.

evaluation of singularity in the Mindlin–Reissner analytical solution and the extended-RKPM solution, the results are compared at a small distance $d = 10^{-4}a$ away from the plate centroid. The comparison of the center deflection obtained with 4×4 , 7×7 , and 9×9 particles shown in Fig. 19 again demonstrates that a coarse mesh can be used in the proposed method to achieve accurate results. A non-uniform discretization of quarter plate with 36 nodes shown in Fig. 20 is also employed. The normalized center deflections obtained using RKPM and Extended-RKPM with respect to the analytical solutions [18] are 0.930 and 0.995, respectively. This calculation demonstrates that the extended RKPM suffers no apparent degradation using non-uniform discretization.

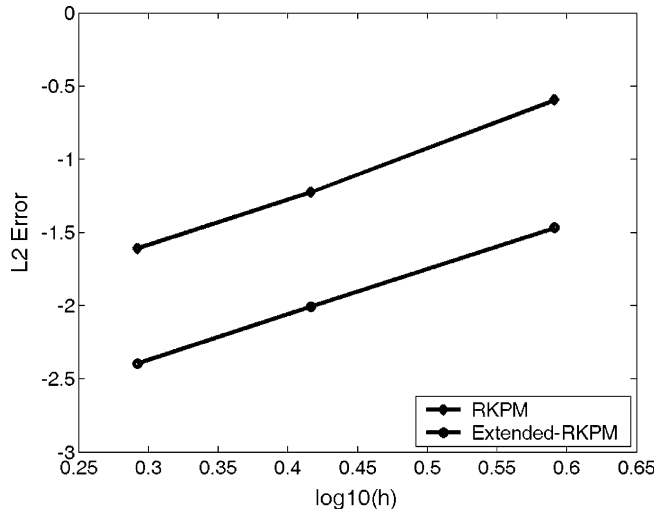


Fig. 17. Error comparison in clamped circular plate problem.

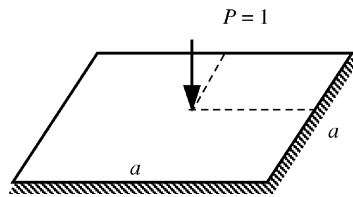


Fig. 18. Clamped square plate subjected to a point load.

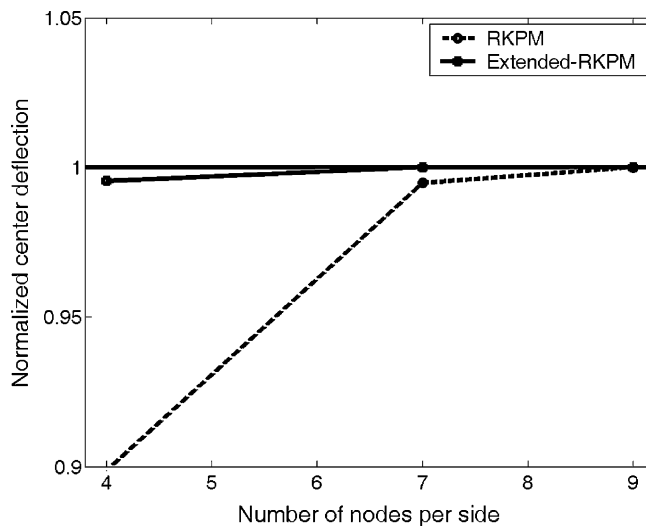


Fig. 19. Center deflection comparison in clamped square plate problem.

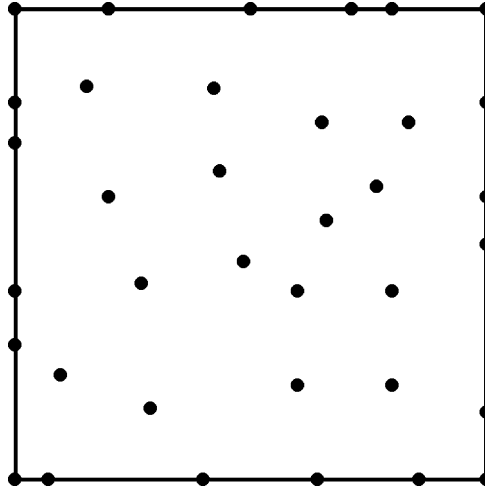


Fig. 20. Non uniform discretization of a quarter of square plate.

6. Conclusions

In this work, an extended meshfree method was presented whose solution consisted of a pair of particular and homogeneous solutions. For the particular solution, an infinite domain was considered. This solution was obtained by integrating the product of a fundamental solution and source term, so that the strong form of the governing equation is satisfied. The original problem is thus reduced to a homogeneous differential equation with boundary conditions modified by the particular solution and its solution was obtained with high precision by the meshfree method when proper reproducing conditions in the meshfree approximation and integration constraints are employed in integrating its weak form. By this separation of the total solution into these two parts, it is possible to effectively solve the homogeneous problem with a fairly coarse discretization of the domain.

Examples on Poisson's equation and the Mindlin–Reissner plate problem were discussed in this paper. For Poisson's equation, the homogeneous solution was solved by introducing a linear basis in the reproducing kernel approximation in conjunction with a stabilized conforming nodal integration to fulfill the linear exactness in the Galerkin approximation of the auxiliary homogeneous problem. In the case of Mindlin–Reissner plate problem, Kirchhoff mode reproducing conditions (KMRC) were introduced in the construction of shape functions for the translational and rotational degrees of freedom of the plate. A stabilized conforming nodal integration that employs curvature smoothing stabilization on the nodally integrated weak form to meet the bending exactness was employed to obtain homogeneous solution of the Mindlin–Reissner plate.

By the proposed method, a significantly enhanced solution accuracy was achieved over the conventional meshfree method in the examples considered. The improvement in accuracy is most dramatic when the source term is localized. Since the particular solution satisfies the strong form, the homogeneous problem enjoys greater computational efficiency since a lower order behavior is involved where a coarse discretization suffices.

Acknowledgements

The support of this work by NSF/DARPA OPAAL Program under grant DMS 98-74015 and General Motors under the grant 17994902 to UCLA is greatly acknowledged. The authors would also like to thank Professor I. Babuska for the valuable discussion on the Mindlin–Reissner plate problem.

References

- [1] T. Belytschko, N. Moës, S. Usui, C. Parimi, Arbitrary discontinuities in finite elements, *Int. J. Numer. Methods Engrg.* 50 (2001) 993–1013.
- [2] T. Belytschko, Y.Y. Lu, L. Gu, Element-free Galerkin methods, *Int. J. Numer. Methods Engrg.* 37 (1994) 229–256.
- [3] C.A. Brebbia, J. Dominguez, *Boundary Elements: An Introductory Course*, Computational Mechanics Publications, McGraw-Hill Book Company, 1989.
- [4] J.S. Chen, C. Pan, C.T. Wu, W.K. Liu, Reproducing kernel particle methods for large deformation analysis of nonlinear structures, *Comput Methods Appl. Mech. Engrg.* 139 (1996) 195–227.
- [5] J.S. Chen, C.T. Wu, S. Yoon, Y. You, A stabilized conforming nodal integration for Galerkin meshfree methods, *Int. J. Numer. Methods Engrg.* 50 (2001) 435–466.
- [6] J.S. Chen, C.T. Wu, S. Yoon, Nonlinear version of stabilized conforming nodal integration for Galerkin meshfree methods, *Int. J. Numer. Methods Engrg.* 53 (2002) 2587–2615.
- [7] J. Dolbow, N. Moës, T. Belytschko, Discontinuous enrichment in finite elements with a partition of unity method, *Finite Elements in Analysis and Design* 36 (2000) 235–260.
- [8] C.A.M. Duarte, J.T. Oden, A h - p adaptive method using clouds, *Comput. Methods Appl. Mech. Engrg.* 139 (1996) 237–262.
- [9] A. Huerta, S. Fernández-Méndez, Enrichment and coupling of the finite element and meshless methods, *Int. J. Numer. Methods Engrg.* 48 (2000) 1615–1636.
- [10] Y. Krongauz, T. Belytschko, EFG Approximation with discontinuous derivatives, *Int. J. Numer. Methods Engrg.* 41 (1998) 1215–1233.
- [11] Y. Krongauz, T. Belytschko, Enforcement of essential boundary conditions in meshless approximations using finite elements, *Comput Methods Appl. Mech. Engrg.* 131 (1996) 133–145.
- [12] S. Li, W.K. Liu, Reproducing kernel hierarchical partition of unity part I: formulation and theory, *Int. J. Numer. Methods Engrg.* 45 (1999) 251–288.
- [13] W.K. Liu, R.A. Uras, Y. Chen, Enrichment of the finite element method with the reproducing kernel particle method, *J. Appl. Mech.* 64 (1997) 861–870.
- [14] W.K. Liu, S. Jun, Y.F. Zhang, Reproducing kernel particle methods, *Int. J. Numer. Methods Fluids.* 20 (1995) 1081–1106.
- [15] J.M. Melenk, I. Babuska, The partition of unity finite element method: basic theory and applications, *Comput. Methods Appl. Mech. Engrg.* 139 (1996) 289–314.
- [16] R. Merle, J. Dolbow, Solving thermal and phase change problems with the extended finite element method, *Comput. Mech.* 28 (2002) 339–350.
- [17] B. Tabarrok, Y. Xiong, Finite element formulations that include particular solutions of governing equations, *Int. J. Numer. Methods Engrg.* 31 (1991) 777–787.
- [18] S.P. Timoshenko, S. Woinowsky-Krieger, *Theory of Plates and Shells*, second ed., McGraw-Hill, New York, 1959.
- [19] G.J. Wagner, W.K. Liu, Hierarchical enrichment for bridging scales and meshfree boundary conditions, *Int. J. Numer. Methods Engrg.* 50 (2001) 507–524.
- [20] D. Wang, J.S. Chen, Locking-free stabilized conforming nodal integration for meshfree Mindlin–Reissner plate formulation, *Comput. Methods Appl. Mech. Engrg.* 193 (2004) 1065–1083. doi:10.1016/j.cma.2003.12.006.
- [21] D. Wang, J.S. Chen, L. Sun, Homogenization of magnetostrictive particle-filled elastomers using an interface-enriched reproducing kernel particle method, *Finite Element in Analysis and Design* 39 (2003) 765–782.
- [22] Y. Wang, *Boundary Elements in Engineering*, China Hydraulic and Hydroelectric Press, Beijing, 1995.